*Int. J. Electrochem. Sci.*, 9 **(2014)** 7003 - 7020

International Journal of
ELECTROCHEMICAL
SCIENCE
www.electrochemsci.org

# In - situ Electrochemical Synthesis, Microscopic and Spectroscopic Characterisations of Electroactive poly(2,5-dimethoxyaniline) – Multi-Walled Carbon Nanotubes Composite Films in Neutral Media

*Milua Masikini, Stephen N. Mailu, Abebaw Tsegaye, Chinwe O. Ikpo, NJagi Njomo, Tesfaye T. Waryo, Priscilla G. L. Baker and Emmanuel I. Iwuoha*[*]

SensorLab, Department of Chemistry, University of the Western Cape Modderdam Road, Bellville 7535, Cape Town, South Africa
[*]E-mail: eiwuoha@uwc.ac.za

*Received:* 18 July 2014 / *Accepted:* 28 August 2014 / *Published:* 29 September 2014

Poly(2,5- dimethoxyaniline)-multi-wall carbon nanotubes (PDMA-MWCNT) nanocomposite films were synthesised by in –situ electrochemical polymerisation. The films were characterised by cyclic voltammetry (CV), ultra–visible spectroscopy (Uv-vis), spectroelectrochemistry, fourier transform infra-red spectroscopy (FTIR) and scanning electron microscopy (SEM). For comparison, Poly(2,5-dimethoxyaniline) without carbon nanotubes (PDMA) was also synthesised. The UV-vis indicated that the films were still in their salt form (doped) and the energy band gap shows the films were semiconductors. The spectroelectrochemistry reveals that the band at 470 nm was found to be bathochromically shifted to 500 nm for potentials below +150 mV (form -750 to 0 mV versus Ag/AgCl) and was found to decrease shifted toward lower energy (red shift or bathochromic shift) with apparition of a new band at around 800 nm with increasing potentials (from +150 to +750 mV versus Ag/AgCl). FTIR confirmed the incorporation of MWCNT into polymer matrix. SEM micrograhs of PDMA and PDMA-MWCNT composite films showed net structure of 'Flower-like'microfiber with diameters ~ 200 nm. The cyclic voltammetry showed two distinctive peaks, which indicates that the films were electoractives in phosphate buffer saline (PBS).

**Keywords:** poly(2,5- dimethoxyaniline)-multi-wall carbon nanotubes, multi-wall carbon nanotubes, poly(2,5-dimethoxyaniline), spectroelectrochemistry and electroactive.

## 1. INTRODUCTION

Since their discovering in 1991 by the Japanese Sumio Iijima during the arc-evaporation synthesis of fullerenes [1,2], carbon nanotubes (CNTs) have generated great interest for several

applications due to their unique structural, electronic, chemical and mechanical properties that make them a very attractive material for a wide range of applications [2-4].

Carbon nanotubes are built from $sp^2$ carbon units, having a diameter measuring on the nanometer scale and micrometer in length, and present a seamless structure with hexagonal honeycomb lattices [4,5]. Typical sizes for CNTs are an inner diameter of 1-3 nm and an outer diameter of approximately 10 nm. Compare to other fibre materials carbon Nanotubes show a unique combination of stiffness, strength, and tenacity which usually shortage one or more of these properties. Their thermal and electrical conductivity are also higher than other conducting materials. They are categorized in two groups basing on their structures, multiwall (MWCNTs) and single-wall (SWCNTs) carbon nanotubes [2,4,6,7]. A single-wall carbon nanotube (SWCNT) consists of a single graphite sheet rolled seamlessly defining a cylinder of 1–2 nm diameters. In SWCNT, there are infinite possibilities in the type of carbon tube and each nanotube which exhibit distinct physical properties. The multiwall carbon nanotubes (MWCNT) consist of a stack of graphite sheets rolled up into concentric cylinders and closed graphite tubules with multiple layers of graphite sheets that define a hole typically from 2 to 25 nm spacing by a distance of approximately between 0.3 and 0.4 nm In general, the MWCNT is considered as a mesoscale graphite system, while the SWCNT is as a single large molecule.

Polyaniline (PANI) has been studied extensively as an important conducting material due to its promising electronic and optical properties [8,9]. It has also generated considerable interest because of the many pathways to its production, its chemical stability, good environmental stability, low cost, and ease of synthesis and ease of redox doping [10]. The continuous growing interest in the study of PANI is caused by these diverse, unique properties and its promising potential in commercial applications. The applications of PANI including in anti-corrosive coatings such as paint, antistatic protection, electromagnetic, secondary batteries; and in electro-optic devices such as liquid crystal devices and photocells and electrochemical biosensors [8,9,11]. Processing of polyaniline into useful products has been problematic because of its insolubility in common non-toxic organic solvents and the fact that it decomposes before melting. Although PANI boasts good environmental stability and conductivity, but it has also facile synthetic routes for preparation. Polyaniline is unique among inherently conducting polymers such as polypyrroles and polythiophenes and differs from them due to its N heteroatom which can participate directly in the polymerization process and also participates in the conjugation of the conducting form of the polymer to a greater extent than the N and S heteroatoms in Polypyrrole and polythiophene. In addition, PANI can be rapidly converted between base and salt forms by treatment with acid or base. PANI or its derivatives can be synthesized by either chemical or electrochemical oxidation of aniline under acidic conditions. The electrochemical synthesis is preferred to chemical synthesis because of its thin films and better ordered polymers.

Extensive research on several conjugated polymers including poly(*p*-phenylene), polyaniline (PANI), polypyrrole (PPY), polythiophene (PT), polyfluorene (PF), poly(*p*-phenylenevinylene) (PPV), and their substituted derivatives have led to their applications in rechargeable batteries, microelectronics, sensors, electrochromic displays, and light-emitting and photovoltaic devices [12]. On the other hand, discovery of carbon nanotubes (CNTs) has led to an explosion of research in nanoscience and nanotechnology. Thus, interest of scientists in nanoscience has since shifted from

synthesis to applications and research of new combinations of the existing materials as hybrid materials, blends and nanocomposites, and exploitation of their complementary properties [13,14]. In this context, development of conducting polymer–CNT composites as novel futuristic materials has been a new focus, because applications of the two constituent offer the possibility to observe synergetic effects. Some studies have been reported in the literature showing that certain discrete properties of the components of conjugated polymer–CNT composites are enhanced, therefore validating their high suitability for some technological applications [15,16].

The various methodologies have been developed for preparing PANI–CNT composites but the common preparative methods are direct solid-state mixing [17] and dispersal of CNTs in PANI solutions [18,19], for both chemical and electrochemical procedures [12]. These preparation methods can be done either by direct mixing or in situ. The in situ polymerisation of aniline or substituted aniline in an acidic dispersion of multi-walled or single-walled carbon nanotubes in the presence of an oxidant at low temperature is the simplest methods among different methods reported [12,20,21]. This last approach has been used in the work for the electrochemical polymerization of PDMA-MWCNT composite. There are also various possibilities of interactions between PANI and CNT in the composites. One of the first suggestions has been the attachment of aniline radicals, generated during electrochemical oxidative polymerization, onto the CNT lattice especially at defect sites [12]. However, the carboxylic sites at the acid-treated CNT are the most likely sites of interaction with aniline monomer [22]. Electrical, thermal, and mechanical properties observed in PANI–CNT composites are intermediate between pure PANI and CNT, and depending on CNT content and the extent of its integration with PANI. Thus, electrochemical properties of PANI-CNT composite are enhanced compare to the two individual components. For instance, electrochemical growth, redox and capacitive currents of the composites values obtained are several-fold higher than the pure PANI onto the electrode [12,22]. The same behaviour is also observed in composites of CNT with substituted PANI derivatives, but the extent of the current increase depends on the nature of the substituent present in the aniline ring [12]. Such a remarkable current enhancement appears to be unique to PANI–CNT composites and has not been observed for any other conjugated polymer–CNT composites.

## 2. EXPERIMENTAL

### *2.1. Chemical and reagents*

The 2,5-Dimethoxyaniline (98%), purchased from Aldrich and fluka. Home grown carbon nanotubes (CNTs; diameter of 40-200 nm and length up to 20 μm; synthesized according to Ndungu et al. method [23]. Hydrochloric acid (HCl), Basic salts including, $NaH_2PO_4$, $Na_2HPO_4$ and KCl used in the preparation of 0.1 M phosphate buffer saline containing 0.1 M KCl at pH 7.4 (PBS) were received from Sigma-aldrich (SA). All other chemicals were of analytical grade, and deionized water (18.2 MΩ cm) purified by a Milli-Q$^{TM}$ system (Millipore) was used as the reagent water for aqueous solution preparation and analytical grade argon (Afrox, South Africa) was used to degas the system.

*2.2. Instrumentation*

Electrochemistry experiments were carried out with a BASi Epsilon –Ec-ver.2.00.71_XP electrochemistry work station for cyclic voltammetry (CV) and electrochemical impedance spectroscopy (EIS) measurements were recorded with Zahner IM6ex Germany using electrodes from BioAnalytical systems, BAS, US in three-electrode electrochemical cell. Impedimetric data and voltammograms for all electrochemical experiments were recorded with a computer interfaced to the Zahner and the BASi Epsilon electrochemical workstation. Glassy carbon elctrodes (GCE) of area 0.071 $cm^2$ and 3 mm of diameter was used as a working electrode. A platinum wire from Sigma Aldrich and Ag/AgCl electrodes from BAS were used as auxiliary and reference electrodes, respectively. Alumina powders and microcloth pads were obtained from Buehler, IL, US and were used for the polishing of the GCE.

The UV-vis spectra were recorded on a Nicolet Evolution 100 Spectrometer (Thermo Electron Corporation, UK). After electropolymerisation of 2,5-dimethoxyaniline (DMA) in the absence and the presence of carbon nanotubes. The samples were dissolved in DMF, placed in 4 $cm^3$ quartz cuvettes and their UV-vis spectra recorded. The spectra were recorded in the region of 200-1100 nm.

FTIR spectra were recorded in the range 4000-300 $cm^{-1}$ using a Perkin Elmer model Spectrum 100 series. The specimen for PDMA and PDMA-MWCNT were prepared by first electrodepositing onto glassy carbon electrode surface, followed by scrapping them gently from the glassy carbon electrode surface.

Raman measurements of MWCNT were carried out with Raman spectrometer (LabRam HR by Jobin-Yvon Horiba scientific Explora, France with a 1200 lines $mm^{-1}$ grating) coupled to a microscope (Model BX41, Olympus). The excitation of Raman scattering was operated with a laser at a wavelength of 532 nm. The laser beam was focused on the sample by means of an x 100 microscope objective. The samples were prepared by drop coating 20 μL of suspension of multi-wall carbon nanotubes on glass slides followed by drying in air at room temperature.

Scanning electron microscopy was used to characterize the surface morphology of MWCNT, PDMA and PDMA-MWCNT. The images were recorded using a Zeiss Auriga HRSEM analyzer using the secondary electron (SE) mode with interchangeable accelerating voltages of 25 kV, and a maximum resolution of 20 μm. The SEM samples for PDMA and PDMA-MWCNT were prepared by electrodeposition onto screen printed carbon electrodes.

*2.3 Purification of carbon nanotubes*

MWCNTs were first purified according to the procedure developed by Liu et al [24]. Briefly, 50 mg of MWCNT was added to 100 mL of an acid mixture of 3:1 concentrated sulphuric acid and concentrated nitric acid. The MWCNTs were sonicated in a DC 200 H ultrasonic cleaner (mrc) for 8 h. The purified nanotubes were filtered using a Millipore sucking filtration system with Whatman filter paper (0.2 μm) and washed with water until the pH tested neutral. The washed MWCNTs were vacuum dried overnight at 50 ºC.

*2.4 Preparation of DMA-MWCNT solution*

A fresh sample (5mg) of the treated MWNTs was dispersed in 2.5 mL of aqueous HCl solution (1M) and sonicated for 5 min, forming then a stable black aqueous colloid (2 mg $mL^{-1}$). Aliquots of 100, 200, 400 and 500 μL of MWCNT colloids were poured into four different vials containing each 5 mL aqueous colloids of DMA and immediately shaken to ensure sufficient mixing and finally after electropolymerisation of MWCNT-PDMA composites with different MWCNT contents (0.1%, 0.5%, 1.0%, 2%, and 4%) were obtained.

*2.5 Electrochemical synthesis of poly(2,5- dimethoxyaniline) multi-walled carbon nanotubes composite modified glassy carbon electrode.*

Before the electro-synthesis of PDMA-MWCNT on the working glassy carbon electrode surface electrode was preconditioned as follows, the GCE was first polished using 0.3 and 0.05 mm alumina slurries and then rinsed with distilled water. The electropolymerisation solution was prepared by mixing 0.1 M of 2,5-dimethoxyaniline (DMA) in 1.0 M HCl (5 mL) and MWCNT (100 μL) or in absence of MWCNT and the mixture was degassed with argon gas for 10 min before electropolymerisation. Doped 2,5-dimethoxyaniline or undoped was polymerized on the surface of GCE by scanning the working electrode potential repeatedly between -200 and +900 mV for 10 cycles at a scan rate of 50 mV/s. The PDMA-MWCNT and PDMA-modified GCE prepared will be denoted as GCE/PDMA-MWCNT and GCE/PDMA, respectively. The same electrochemical synthesis procedure was employed for the deposition of the polymer on screen printed carbon electrodes (SPCE) for SEM analysis and on indium tin oxide electrodes (ITO) for spectroelectrochemistry.

## 3. RESULTS AND DISCUSSION

*3.1 Electrochemical synthesis of PDMA-MWCNT composite*

Electrochemical polymerization of the monomer 2,5-dimethoxyaniline and multi wall carbon nanotubes (MWCNT) on glassy carbon electrode surfaces was achieved by cycling the potential repeatedly 10 cycles between -0.2 and 0.9 V at scan rate of 50 mV $s^{-1}$ (see 2.5). The green emeraldine film on the electrode surface was obtained as a result of polymerization. The polymerization reaction was initiated by the formation of resonance-stabilised aniline radical cations from the protonated 2,5-dimethoxyaniline monomer. During the polymerisation, the peak current increased as the number of cyclic voltammograms increased and also the polymer thickness increased with successive potential cycles. This behaviour indicates that conductive polymeric films are formed. The cyclic voltammograms for the electrodeposition of PDMA-MWCNT films on the glassy carbon electrode surfaces are shown in figures 1. The electrodeposition of PDMA-MWCNT on the glassy carbon electrode surface proceeds via a radical cation mechanism. Two pairs of redox peaks centred at ca. 0.18 V (a/a') and 0.55 V (c/c′), corresponding to transition from leucoemeraldine to emeraldine and

emeraldine to pernigraniline states [25], respectively, were observed for both the doped PDMA and PDMA-MWCNT composite. This indicates the presence of discrete electroactive regions in the films. The origin of another pair of redox peaks observed at ca. 0.43 V (b/b´) for both PDMA-MWCNT and PDMA is much more complex and it can be attributed to many different intermediates and degradation products (cross-linked polymer, benzoquinone, emeraldine/emeraldine radical cation etc.) [26].

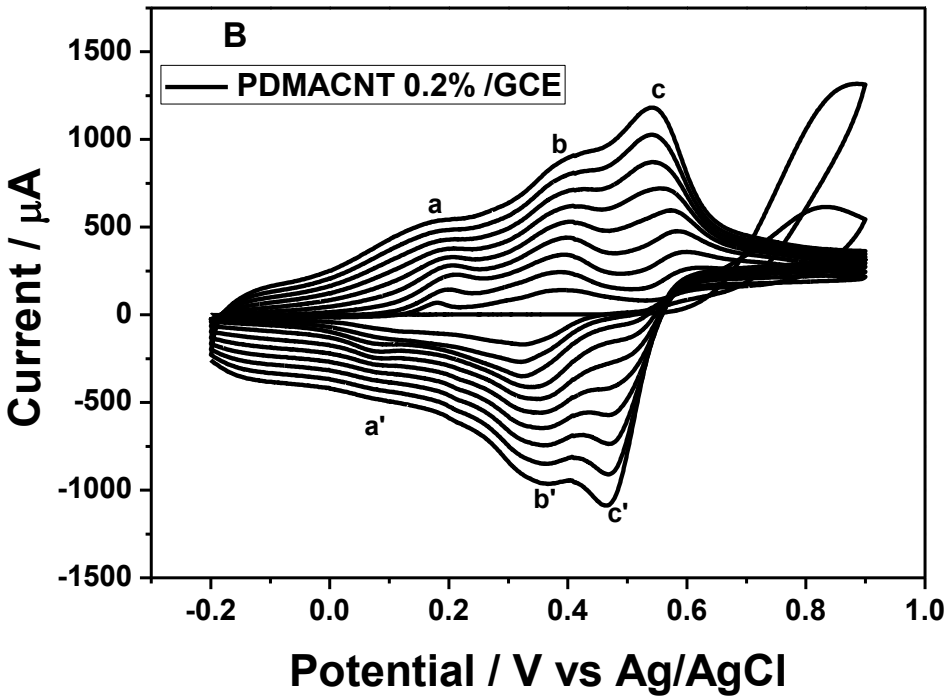


**Figure 1.** Cyclic voltammograms for electrochemical synthesis of PDMA-MWCNT films in 1.0 M HCl at a scan rate of 50 mV $s^{-1}$.

*3.1.1 Optimization of PDMA-MWCNT composite*

The PDMA-MWCNT composite films were formed by electropolymerisation of aniline dissolved MWCNT with different contents. To elucidate the effect of MWCNT on the properties of PDMA films, electrochemical performance of composite films was evaluated by carrying out a CV measurement at scan rate of 2 mV $s^{-1}$ in PBS and at scan rate of 10 mV $s^{-1}$ using HCl solution. Figure 2 (A and B) has shown the cyclic voltammetry behaviour of the PDMA-MWCNT composite films prepared from the growth solution at different scan rates. Figure 2A has presented the films prepared from the growth solutions containing 0, 0.2, 0.4, 0.8 and 1% MWCNTs in 1M HCl solution. The voltammograms have shown that the negative sweeps were very symmetrical to their positive counterparts and this has explained the excellent reversibility of all these PDMA-based films in the high positive potential range. In addition, PDMA-MWCNT composite films showed strong defined peaks, indicating their higher electroactivity over pure PDMA. The same result was observed for the films prepared from the growth solutions containing 0, 0.2, 0.4, 0.8 and 1 % MWCNT and characterised in PBS at scan rate of 2 mV $s^{-1}$ (Fig.2 B).

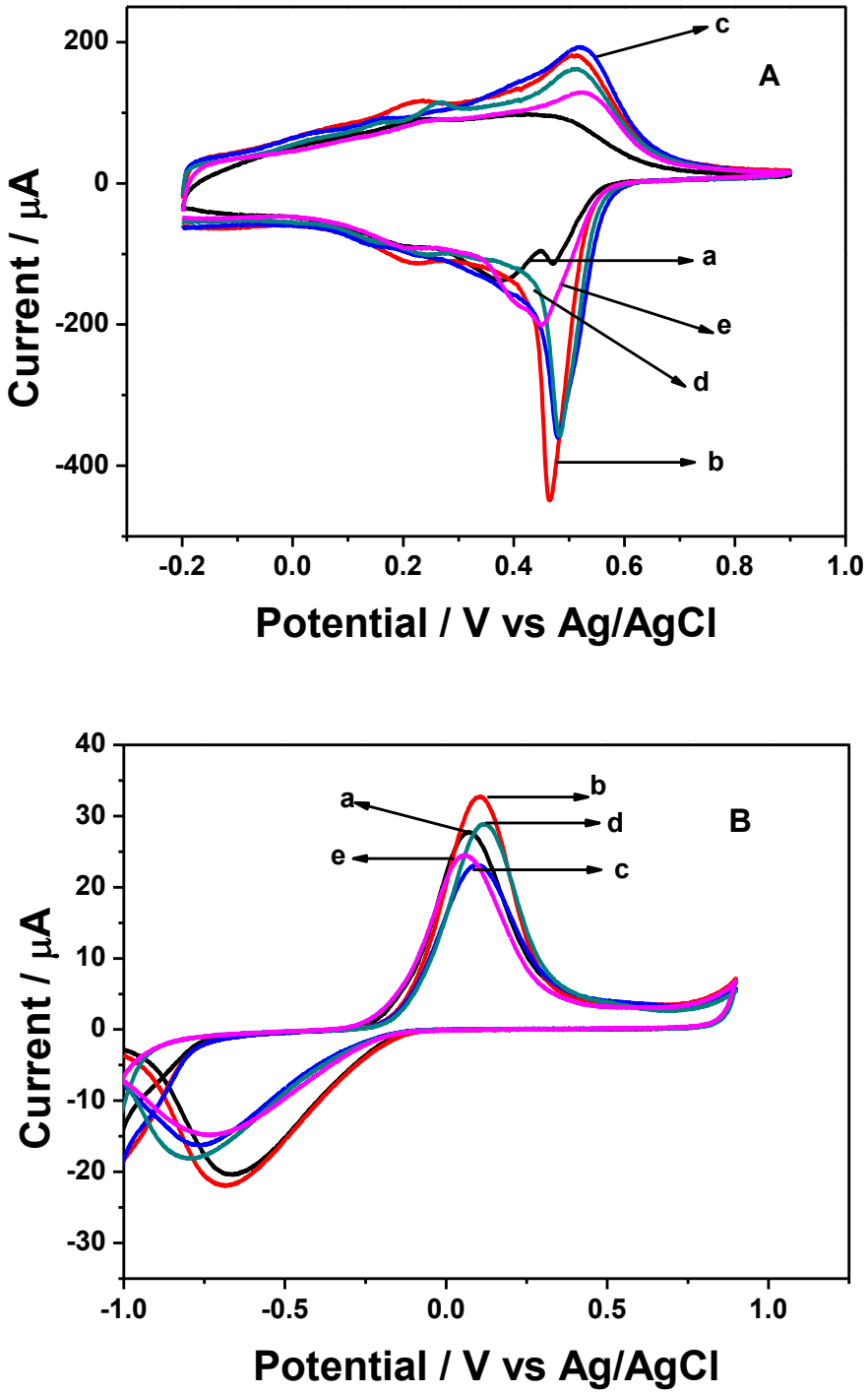


**Figure 2.** Cyclic voltammetric behaviour of the PDMA-MWCNT composite films prepared from the growth solution with 0 (a), 0.2 (b), 0.4 (c) 0.8 (d) and 1 % (d) MWCNT in 1M HCl (A) electrolyte at the scan rate of 10 mV $s^{-1}$ and in PBS (B) at the scan rate of 2 mV $s^{-1}$.

It has been reported in the literature [27,28] that the electrochemical activities of PANI films coincide with the degree of protonation; therefore, a promotion in the protonation with a doping effect of MWCNT on PANI may be expected. The same phenomena occur in our case for PDMA. This can

be explained by the fact that MWCNTs have large π-bonded surface which might interact strongly with the conjugated structure of PDMA via π-stacking, and that the resulting highly conjugated π-system would promote the degree of electron delocalization and then lead to preferential protonation of the amine nitrogen atoms.

Figure 3 (A and B) below has shown also the cyclic voltammetry behaviour of the PDMA and PDMA-MWCNT composite films prepared at different scan rates. Figure 3A has presented the cyclic voltammograms of PDMA film (a) and PDMA-MWCNT composite film prepared from the growth solution with 0.2 % MWCNT (b) in PBS. It can be observed that the larger voltammetric output current occur at the composite film ($I_{pc}$ = 32.68 A and $I_{pa}$ = 21.93 A) compare to the pure PDMA film ($I_{pc}$ = 27.55 A and $I_{pa}$ = 20.43 A) and slight shift on the peak potentials was also observed, PDMA ($E_{pa}$ = -672 mV and $E_{pc}$ = 74 mV) and PDMA-MWCNT ($E_{pa}$ = -683 mV and $E_{pc}$ = 102 mV). Hence, the same observation was obtained when PDMA and PDMA-MWCNT (Fig.3 B) were both run in 1M HCl solution at scan rate of 10 mV $s^{-1}$.

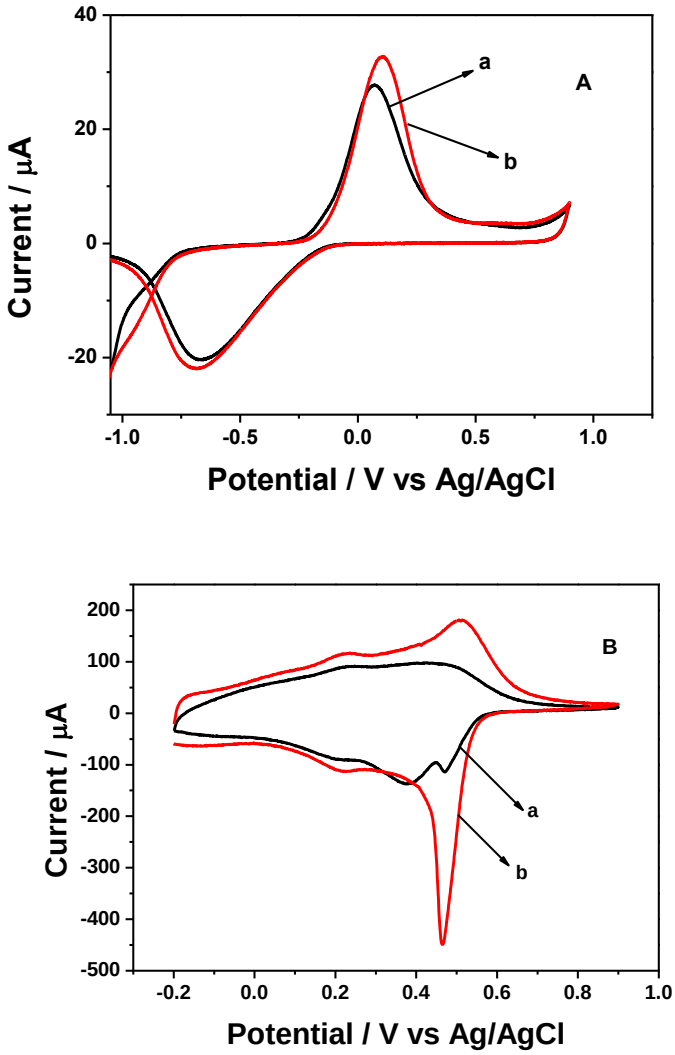


**Figure 3.** Cyclic voltammograms of (a) PDMA and (b) PDMA-MWCNT (0.2%) films in PBS2 (A) at scan rate of 2 mV $s^{-1}$ and in 1M HCl (B) at scan rate of 10 mV $s^{-1}$.

The difference in electrochemical behaviour between the pure PDMA and PDMA-MWCNT composite films was clearly expressed from the two figures above (Fig. 2 and Fig. 3). Thus, PDMA-MWCNT composite film prepared from the growth solution with 0.2 % MWCNT was found to be the optimum ratio and used throughout for the electrochemical synthesis of the PDMA-MWCNT composite since it has higher peak current either in acid or buffer as compared to the others.

### *3.1.2 Electrochemical characterisation of PDM-MWCNT composite*

The electrodeposited PDMA-MWCNT composite film was subjected to characterisation by cyclic voltammetry in the potential range of -900 mV $s^{-1}$ to 900 mV $s^{-1}$ in 0.1 M PBS at various scan rates (30 – 500 mV $s^{-1}$) as shown in figure 4. The CV shows redox behaviour with the anodic peak (a) and the cathodic peak (b) corresponding to the transition of PDMA backbone from its leucoemeraldine state to emeraldine. It was also observed that the peak currents increased with increase in scan rates. These results confirm that PDMA-MWCNT film was successfully attached onto the glassy carbon electrode surface and film in PBS showed that it exhibited good electroactivity at pH 7.4.

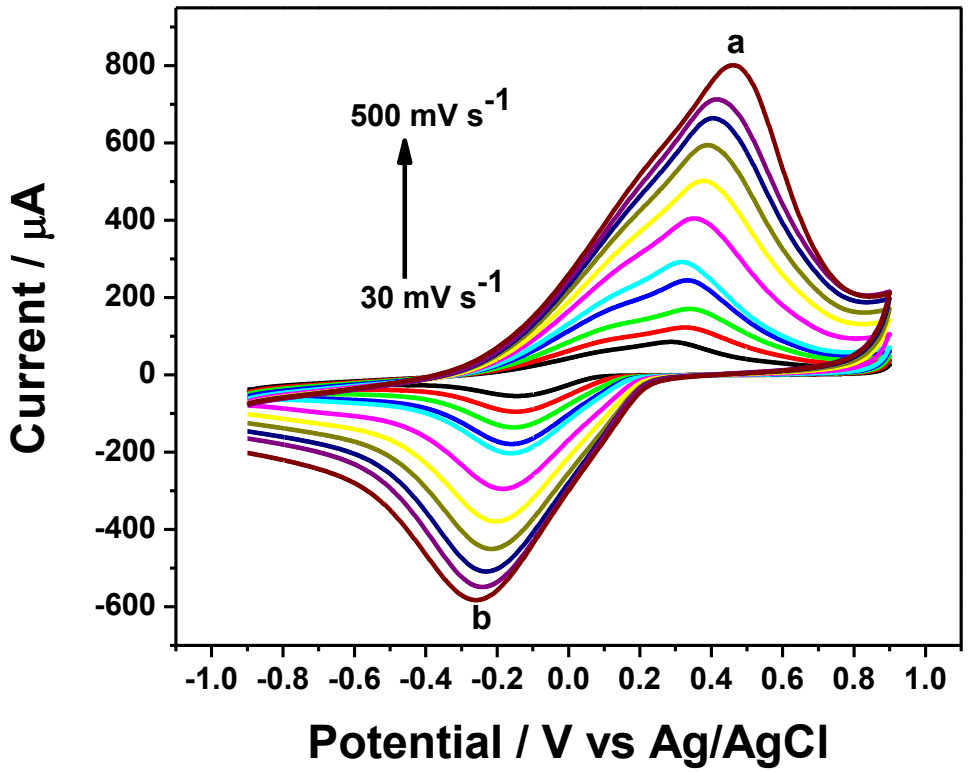


**Figure 4.** Cyclic voltammograms of PDMA-CNT composite in 0.1 M PBS (pH 7.4) at scan rates of 30, 50, 70, 90, 100, 150, 200, 250, 300, 400 and 500 mV $s^{-1}$, respectively.

It was also observed that the cathodic peak potentials do not shift with increase of scan rate meanwhile peak currents increased with scan rate indicating surface–confined electroactive species.

Contrarily, anodic peak potentials shift positively with increase of scan rate indicating that electrons hopping from the solutions to the polymer-multi-walled carbon nanotubes composite.

### *3.2 Ultraviolet–Visible Spectroscopy (UV-vis)*

UV-vis spectroscopy was utilised to understand the electronic states of PDMA and PDMA-MWCNT as shown in figure 5. The UV-Vis results for the PDMA and PDMA-MWCNT materials have shown three sharp distinct absorption bands at the wavelengths 300 (4.1 eV), 360 (3.4 eV), 800 (1.5 eV) nm and small peak at 450 nm, respectively. The peaks at 300 (4.1 eV) nm and 360 (3.4 eV) nm are attributed to the π–π* transition of benzoid rings [29-31]. The peak at 300 nm is characteristic of the leucoemeraldine form of PDMA, while the band at 360 nm is characteristic of the protonated form of emeraldine salt [32]. The band at 800 nm is attributed to polarons (free or mobile) [32] or to polaron-π* band transition [33], which is originate the charged cationic species [34]. The peaks at 360 nm and 450 nm give also an indication that the PDMA is in the salt form (doped).

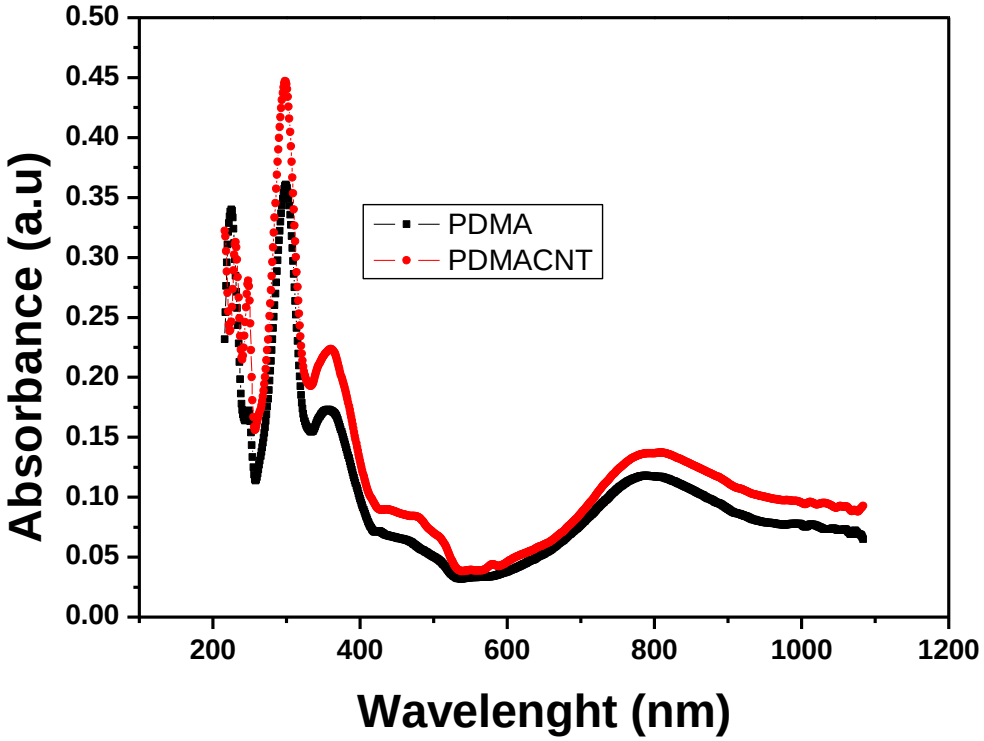


**Figure 5.** UV-visible absorption spectra of PDMA and PDMA-MWCNT in DMSO.

### *3.3 Spectroelectrochemistry Spectroscopy*

The spectroelectrochemistry is a technique that involves simultaneous application of electrochemical and optical spectroscopic techniques to investigate a phenomenon such as

understanding of redox reactions through identification of product and its intermediates. In this study the spectroelectrochemistry was used to monitor the change of PDMA forms by applying potential (anodic sweep). Figure 6 shows UV-vis spectra of ITO/PDMA-MWCNT film at different applied potentials (-750 to +750 mV versus Ag/AgCl) in PBS.

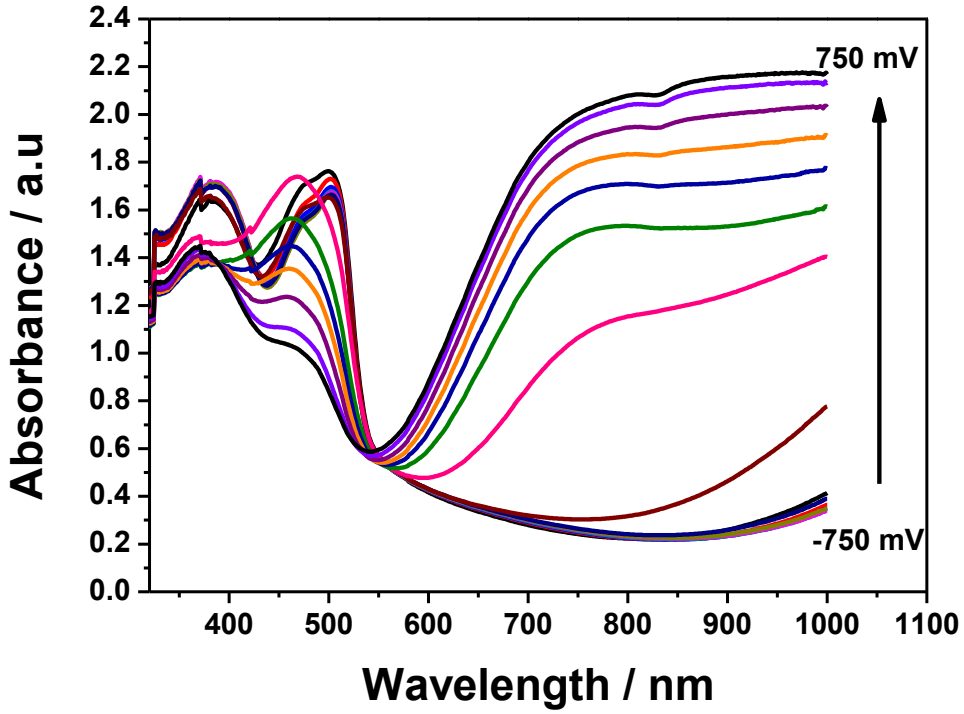


**Figure 6.** UV-vis spectra of PDMA-MWCNT film on ITO electrode recorded at different applied potential (-750 to +750 mV) in PBS.

The film of PDMA-MWCNT has shown two peaks at 380 (3.2 eV) and 500 (2.48 eV) nm in the potential ranges -750 to 0 mV, and three peaks at 370 (3.3 eV), 470 (2.6 eV) and 800 (1.5 eV) nm in the potential range +150 to +750 mV. The band at 380 or 370 nm is often referred to as the 360 nm band correspond to $\pi$ - $\pi^*$ of the benzoid rings which is characteristic of the protonated forms of emeraldine salt of PDMA-MWCNT as explained previously (see section 3.2) while the bands at 470 or 500 nm and 800 nm are due to polarons. The Absorbance at 370 nm and 470 nm represent the transition of emeraldine form of the composite to more oxidized form. In addition, the band at 470 nm decreases with increasing potentials (from +150 to +750 mV versus Ag/AgCl) and was found to be bathochromically shifted to 500 nm for potentials below +150 mV (form -750 to 0 mV versus Ag/AgCl). Increasing the applied potential (from +150 to +750 mV versus Ag/AgCl), the absorbance at 470 nm which was found to decrease shifted toward lower energy (red shift or bathochromic shift) with apparition of a new band at around 800 nm. This band at 800 nm, which increased with increasing of potential at potentials above 0 mV indicating conversion of emeraldine form of the composite to more oxidized (emeraldine state to pernigraniline state) form due to the formation of polarons. At potentials below 0 mV the band at 800 nm was not observed indicating no more conversion occurred.

When PDMA film (figure not shown) was used no much difference was found compare to PDMA-MWCNT film.

*3.4 Fourier Transforms Infra-Red Spectroscopy*

The FTIR was performed in order to study the structural changes in the PDMA after introduction of MWCNT. The FTIR spectra of PDMA and PDMA-MWCNT are shown in figure 7 (A-B). The FTIR spectrum of PDMA Fig. 7(A) exhibits main characteristic bands of PDMA in the 400 – 4000 $cm^{-1}$ range according to the literatures [33,35,36]. A broad and weak band at ~ 3237 $cm^{-1}$ is due to the N–H stretching mode. The peak 1194 $cm^{-1}$ corresponds to the quinoid rings in the polymer backbone. The corresponding stretching vibration bands for the benzenoid rings occur at 1504 $cm^{-1}$ and 1447 $cm^{-1}$. A band at ~ 1120 $cm^{-1}$ is assigned to the plane bending vibration of C–H, which is formed during protonation, the bands at 1028 and 982 $cm^{-1}$ are assigned to the presence of o-methoxy groups in PDMA, and a band at ~ 800 $cm^{-1}$ indicates the ortho-substituted benzene ring. The FTIR spectra of PDMA-MWCNT Fig. 7(B) seems to show the same peaks as in the PDMA with some shifts on the main peaks, which indicated changes of environment at the molecular level. In addition, presence of peaks at ~ 1732, 1364 and 1160 $cm^{-1}$ in the PDMA-MWCNT spectra can be assigned to the C=O stretch, O–H bend and C–O stretch, respectively, corresponding to the stretching mode of the carboxylic acid group (-COOH) [37]. The presence of these peaks which are absent to FTIR spectrum of PDMA indicated presence of MWCNT in PDMA.

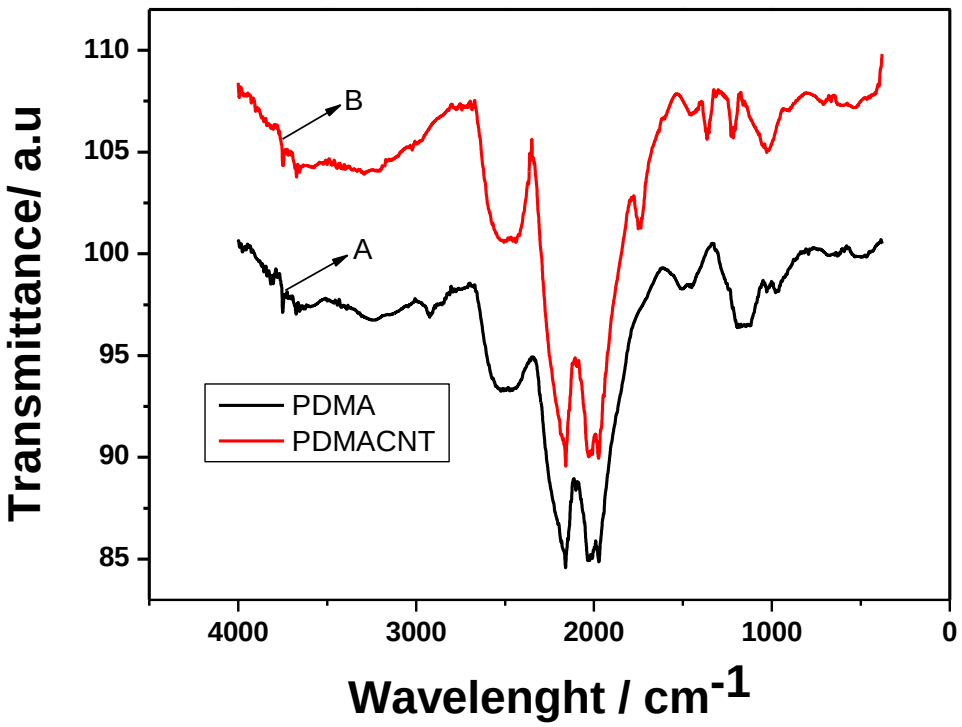


**Figure 7.** FTIR spectra of (A) PDMA and (B) PDMA-MWCNT.

*3.5 Scanning Electron Microscopy*

*3.5.1 PDMA and PDMA-MWCNT*

The surface morphology of PDMA and PDMA-MWCNT films was investigated using SEM as shown in figures 8 and 9. The PDMA film (Fig. 8) presents net structure of 'Flower-like'microfiber with diameters ~ 200 nm and it is not very uniform. The PDMA-MWCNT (Fig. 9) composite film also shows net structure of microfiber, but the pore is smaller and denser. Thus, the film is more uniform, no agglomerations and porous due to the interaction between PDMA nonofibers and MWCNTs.

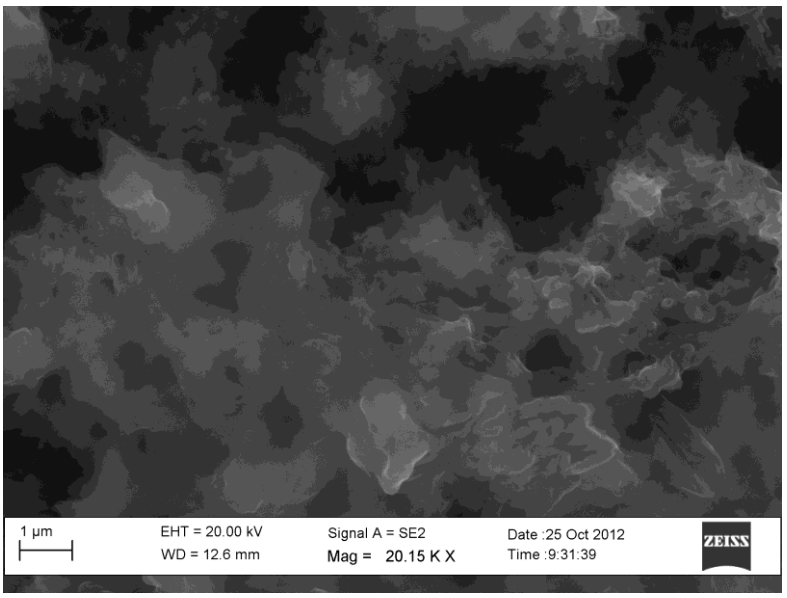


**Figure 8.** SEM image of PDMA

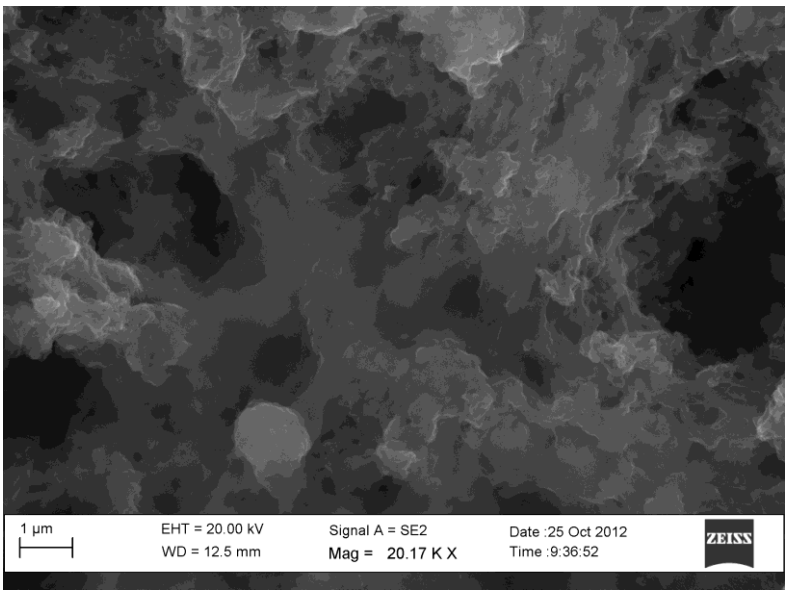


**Figure 9.** SEM images of PDMA-MWCNT

*3.5.2 MWCNT*

Prior to any used of MWCNT, the as received MWCNTs were purified by acid-treatment to render them soluble for further characterisation and application. The acid treatment process should be carried out with precaution, since treating agent can destroy relevant bonds located on surfaces and chemical groups resulting to the existence of physical defects on the side wall of MWCNTs [38]. Figures 10 and 11 show the HRTEM images of as received and purified MWCNTs, respectively. The image on figure 10 revealed several layers of graphitic carbon and hollow cores [39]. In addition, in as received MWCNTs a number of physical defects on the side wall are hardly observed and bending tubes were observed which caused agglomeration [40]. In comparison with as-received CNTs, acid treated CNTs in figure 11 shows a decrease in the outer diameter of the tubes with increased surface roughness. Furthermore, the MWNTs were stretched leading to the good dispersion and less defects on the side wall is observed [40].

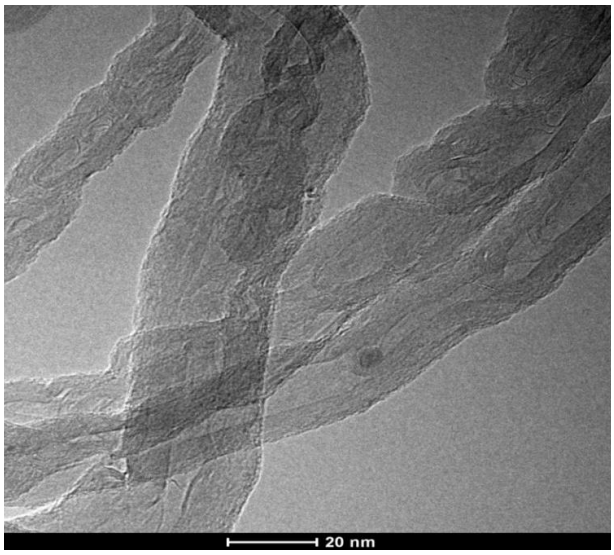


**Figure 10.** HRTEM micrograph of MWCNTs as received.

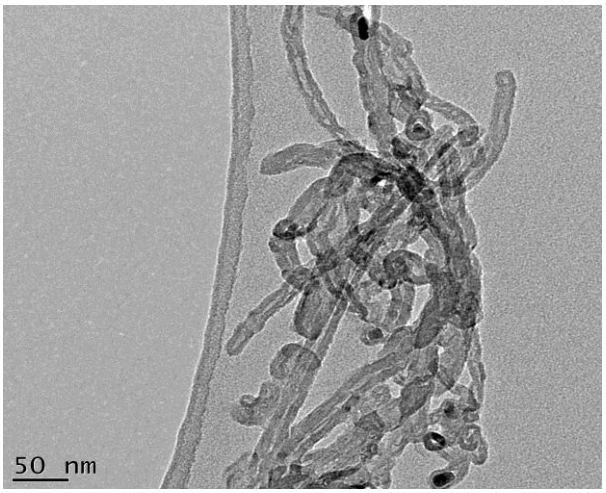


**Figure 11**. HRTEM micrograph of acid-purified MWCNTs.

*3.6 Raman spectroscopy of MWCNT*

Raman spectroscopy is a popular non-destructive technique effectively used in the micro-structural characterisation of carbon based materials. The well-known Raman spectrum of diamond has a single Raman active mode at 1332 $cm^{-1}$ while the Raman spectrum of single crystal graphite consists of a narrow peak at 1580 $cm^{-1}$ and is named 'G' for graphite. For MWCNTs two major narrow bands exists, G band for graphite as mentioned above located 1580 – 1600 $cm^{-1}$ which is associated with the $E_{2g}$ mode and a second band located at 1350 $cm^{-1}$ which is associated with the $A_{1g}$ mode and becomes active in the presence of disorder, thus, is named 'D' for disorder [41].

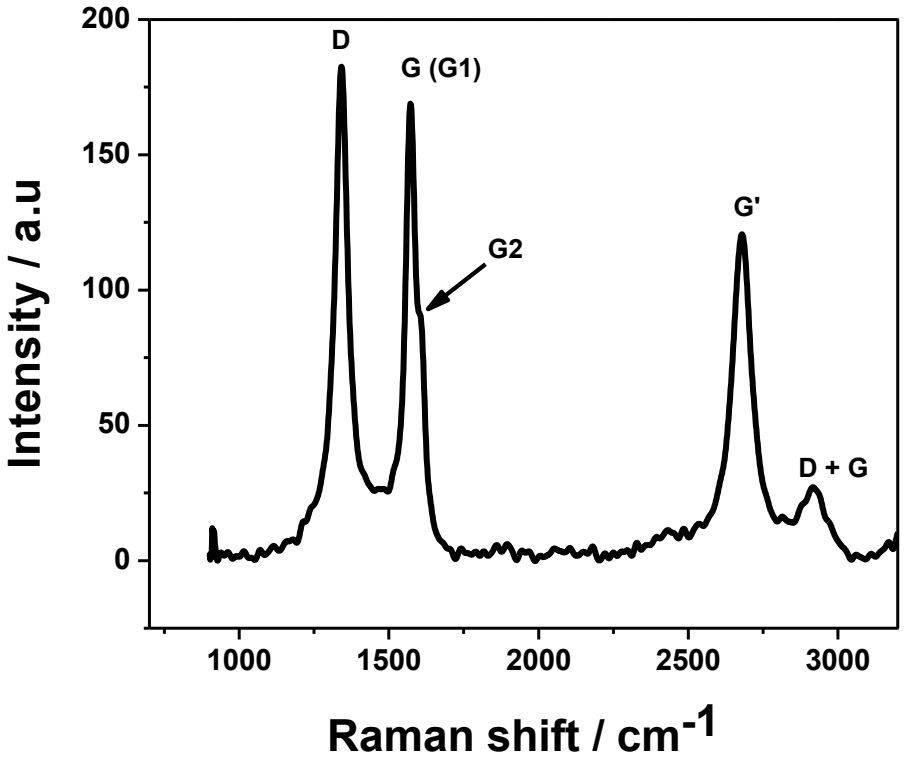


**Figure 12.** Raman spectra of MWCNTs treated by $HNO_3/H_2SO_4$.

Figure 12 shows Raman spectra of acid treated MWCNTs in which three dominating features are observed. The two sharp Raman peaks showing the characteristic of CNTs, the defects of the structure, named D (disorder) band at 1338.60 $cm^{-1}$ and another bands point is the graphite band at 1574.05 $cm^{-1}$, named G band. The third band at 2683.56 $cm^{-1}$ is attributed to second-order harmonic (the G' band). Additionally, a small feature called G2 or D' near graphite band (1616.25 $cm^{-1}$) and another distinguishable feature like D+G band at 2919.01 $cm^{-1}$, are also observed. The D and G bands observed in the Raman spectra of the acid treatment of MWCNTs (Fig. 12), indicates that the acid treatment does not destroy the structure of CNT [38,40]. In addition, *G* peak corresponds to the tangential stretching ($E_{2g}$) mode of highly oriented pyrolytic graphite (HOPG), which indicates the presence of crystalline graphitic carbon in the CNTs and *D* peak can be attributed to the disorder

induced features due to defect and finite particle size effect [41]. The tangential G-band at ~1580 $cm^{-1}$, resulting from the graphite-like in-plane mode, can be split into several modes but only two are the most distinct and are also observed in figure 13: G1 band at 1574.05 $cm^{-1}$ and G2 at 1616.25 $cm^{-1}$. This result has been also reported in literatures [42-44]. These bands are related to the lattice vibration of all carbon materials with sp2 bonds. The ratio of the intensity of *D* peak ($I_D$) to the intensity of *G* peak ($I_G$) is used to measure the amount of disorder in the CNTs [45]. The $I_D/I_G$ ratio of the MWCNTs in this experiment is ~ 1, which suggests less defect content in the acid treated MWCNTs.

## 4. CONCLUSIONS

In this work, it can be concluded that Poly(2,5- dimethoxyaniline)-multi-wall carbon nanotubes (PDMA-MWCNT) nanocomposite films were synthesised by in –situ electrochemical polymerisation. The polymers synthesized in the absence and presence multi-wall carbon nanotubes exhibited quinoid and benzoid bands typically of polyaniline FTIR-spectra which confirmed the polymers were formed. The presence of the carboxylic acid group suggested that MWCNT was incorporated into the polymer backbones. Besides, UV-vis bands and spectroelectrochemistry shifts also showed that MWCNT was incorporated into the polymer backbones. SEM micrograph of the PDMA-MWCNT composite film showed net structure of microfiber with smaller pore s and denser. Consequently, the film is more uniform, no agglomerations and porous due to the interaction between PDMA nonofibers and MWCNTs. The Spectroelectrochemistry showed bathochromic shift. Cyclic voltammetric characterisation of the films showed two redox peaks, which prove that the composite films on the electrode were electroactive and conductive and exhibit reversible electrochemistry. These results prove that the composite can be a promising material for development of novel electro-catalysts for use in sensor and supercapacitor devices.

## Reference

1 S. Iijima, *Nature.* 354 (1991) 56-58.
1. A. Merkoçi, *Microchimica Acta.* 152 (2006) 157-174.
2. R.H. Baughman, A.A. Zakhidov, W.A. de Heer, *Science.* 297 (2002) 787-792.
3. G.A. Rivas, M.D. Rubianes, M.C. Rodríguez, N.F. Ferreyra, G.L. Luque, M.L. Pedano, S.A. Miscoria, C. Parrado, *Talanta.* 74 (2007) 291-307.
4. Q. Zhao, Z. Gan, Q. Zhuang, *Electroanalysis.* 14 (2002) 1609-1613.
5. M.S. Dresselhaus, Y.M. Lin, O. Rabin, A. Jorio, A.G. Souza Filho, M.A. Pimenta, R. Saito, G.G. Samsonidze, G. Dresselhaus, *Materials Science and Engineering C.* 23 (2003) 129-140.
6. K. Balasubramanian, M. Burghard, *Small.* 1 (2005) 180-192.
7. M. Gerard, A. Chaubey, B.D. Malhotra, *Biosensors and Bioelectronics.* 17 (2002) 345-359.;
8. M. Kraljić, Z. Mandić, L. Duić, *Corrosion Science.* 45 (2003) 181-198.
9. D. Zhang, Y. Wang, *Materials Science and Engineering: B.* 134 (2006) 9-19.
10. M.C. Bernard, G.A. Hugot-Le, S. Joirets, P.V. Phong, *Synthetic Metals.* 119 (2001) 283-284.
11. P. Gajendran, R. Saraswathi, *Pure and Applied Chemistry.* 80 (2008) 2377-2395.
12. J. Anand, S. Palaniappan, D.N. Sathyanarayana, *Progress in Polymer Science (Oxford).* 23 (1998) 993-1018.

13. A. Pud, N. Ogurtsov, A. Korzhenko, G. Shapoval, *Progress in Polymer Science.* 28 (2003) 1701-1753.
14. M. Baibarac, P. mez-Romero, *Journal of nanoscience and nanotechnology.* 6 (2006) 289-302.
15. L. Dai, *Australian Journal of Chemistry.* 60 (2007) 472-483.
16. I.A. Tchmutin, A.T. Ponomarenko, E.P. Krinichnaya, G.I. Kozub, O.N. Efimov, *Carbon* 41 (2003) 1391-1395.
17. M. Baibarac, I. Baltog, S. Lefrant, J.Y. Mevellec, O. Chauvet, *Chemistry of Materials.* 15 (2003) 4149-4156.
18. X.-b. Yan, Z.-j. Han, Y. Yang, B.-k. Tay, *The Journal of Physical Chemistry C.* 111 (2007) 4125-4131.
19. M. Cochet, W.K. Maser, A.M. Benito, M.A. Callejas, M.T. Martinez, J.-M. Benoit, J. Schreiber, O. Chauvet, *Chemical Communications.* (2001) 1450-1451.
20. M.R. Karim, C.J. Lee, Y.-T. Park, M.S. Lee, *Synthetic Metals.* 151 (2005) 131-135.
21. P. Gajendran, R. Saraswathi, *The Journal of Physical Chemistry C.* 111 (2007) 11320-11328.
22. P. Ndungu, A. Nechaev, L. Khotseng, N. Onyegebule, W. Davids, R. Mohammed, G. Vaivars, B. Bladegroen, V. Linkov, *International Journal of Hydrogen Energy.* 33 (2008) 3102-3106.
23. J. Liu, A.G. Rinzler, H. Dai, J.H. Hafner, R.K. Bradley, P.J. Boul, A. Lu, T. Iverson, K. Shelimov, C.B. Huffman, F. Rodriguez-Macias, Y.-S. Shon, T.R. Lee, D.T. Colbert, R.E. Smalley, *Science.* 280 (1998) 1253-1256.
24. A. Morrin, O. Ngamna, A.J. Killard, S.E. Moulton, M.R. Smyth, G.G. Wallace, *Electroanalysis*. 17 (2005) 423-430.
25. S-Y. Hong, Y.M. Jung, S.B. Kim, S-M. Park, *The Journal of Physical Chemistry B.* 109 (2005) 3844-3850.
26. A.F. Diaz, J.A. Logan, *Journal of Electroanalytical Chemistry and Interfacial Electrochemistry.* 111 (1980) 111-114.
27. T. Kobayashi, H. Yoneyama, H. Tamura, *Journal of Electroanalytical Chemistry and Interfacial Electrochemistry.* 177 (1984) 281-291.
28. E.I. Iwuoha, S.E. Mavundla, V.S. Somerset, L.F. Petrik, M.J. Klink, M. Sekota, P. Bakers, *Microchimica Acta.* 155 (2006) 453-458.
29. M.J. Klink; E.I. Iwuoha, E.E. Ebenso, *International Journal of Electrochemical Science.* 6 (2011) 2429 - 2442.
30. M.J. Klink, E.I. Iwuoha, E.E. Ebenso, *International Journal of Electrochemical Science.* 7 (2012) 3031 - 3046.
31. A.A. Nekrasov, V.F. Ivanov, A.V. Vannikov, *Journal of Electroanalytical Chemistry.* 482 (2000) 11-17.
32. N. Njomo, T. Waryo, M. Masikini, C.O. Ikpo, S. Mailu, O Tovide, N. Ross, A. Williams, N. Matinise, C.E. Sunday, N. Mayedwa, P.G.L. Bakera, K.I. Ozoemena, E.I. Iwuoha, *Electrochim. Acta*. (2014), http://dx.doi.org/10.1016/j.electacta.2013.12.150.
33. , S. Shreepathi R. Holze, *Chemistry of Materials.* 17 (2005) 4078-4085.
34. S.E. Mavundla, G.F. Malgas, P.G.L. Baker, E.I. Iwuoha, *Electroanalysis*. 20 (2008) 2347-2353.
35. H. Zhong, R. Yuan, Y. Chai, W. Li, X. Zhong, Y. Zhang, *Talanta* 85 (2011) 104-111.
36. O-K Park, T. Jeevananda, N.H. Kim,S-il. Kim, J.H. Lee, *Scripta materialia.* 60 (2009) 551-554.
37. A.G. Osorio, I.C.L. Silveira, V.L. Bueno, C.P. Bergmann, *Applied Surface Science.* 255 (2008) 2485-2489.
38. Q. Zeng, Z. Li, Y. Zhou, *Journal of Natural Gas Chemistry.* 15 (2006) 235-246.
39. K. Chokchai, W. Papitchaya, C. Thanawee, P. Wisanu, *Journal of the Microscopy Society of Thailand.* 24 (2010) 133-135.
40. M. Ashish, T. Mark, S.R. Susanta, P.D. Maguire, J.A. McLaughlin, *Journal of Nanoscience and Nanotechnology.* 9 (2009) 4392-4396.

41. A.M. Rao, E. Richter, S. Bandow, B. Chase, P.C. Eklund, K.A. Williams, S. Fang, K.R. Subbaswamy, M. Menon, A. Thess, R.E. Smalley, G. Dresselhaus, M.S. Dresselhaus, *Science.* 275 (1997) 187-191.
42. G.S. Duesberg, I. Loa, M. Burghard, K. Syassen, S. Roth, *Physical Review Letters.* 85 (2000) 5436-5439.
43. M. Zdrojek, W. Gebicki, C. Jastrzebski, T. Melin, A. Huczko, *Solide State Phenomena.* 99 (2004) 265-268.